The Importance of a Moving Boundary Approach for Modeling the SEI Layer Growth to Predict Capacity Fade

Journal of The Electrochemical Society, 2022 **169** 040548

The Importance of a Moving Boundary Approach for Modeling the SEI Layer Growth to Predict Capacity Fade

Maitri Uppaluri,[1] Krishna Shah,[2,3] Vilayanur Viswanathan,[4] and Venkat R. Subramanian[2,*,z]

[1]*Materials Science and Engineering Program, Texas Materials Institute, The University of Texas at Austin, Austin, Texas 78712, United States of America*
[2]*Walker Department of Mechanical Engineering & Material Science Engineering, Texas Materials Institute, The University of Texas at Austin, Austin, Texas 78712, United States of America*
[3]*Department of Mechanical Engineering, University of Alabama, Tuscaloosa, Alabama 35401, United States of America*
[4]*Energy & Environment Division, Pacific Northwest National Laboratory, Richland, Washington 99352, United States of America*

One of the contributing factors to the aging of lithium-ion batteries is the growth of the solid-electrolyte interphase (SEI) layer. The growth of the SEI layer leads to the irreversible loss of lithium available for cycling and increases the resistance of the battery. Physics-based models in literature model the kinetically limited or solvent diffusion-limited growth. In such models, the interface resistance is a constant, and the contribution to the overpotential of the intercalation reaction from the SEI layer is considered to be ohmic. In this study, we propose a model that describes the growth of the SEI layer on the electrode surface as a moving interface. The transport of lithium ions and the solvent in the electrolyte are affected by this moving interface. The equations that govern the species transport and the potential drop across the SEI layer are derived from dilute solution theory and solved by transforming the coordinates of the moving boundary. The ion transport induces changes in the conductivity across the SEI layer, which affects the potential drop that arises due to its growth. The effects of this potential on capacity fade are studied over cycling the battery.
 [DOI: 10.1149/1945-7111/ac65b6]

Manuscript submitted January 11, 2022; revised manuscript received March 14, 2022. Published April 25, 2022. *This paper 984, was presented during the 239th Meeting of the Electrochemical Society, May 30—June 3, 2021.*

List of symbols

a	Surface area per volume of electrode
c	Electrolyte concentration
c_s	Solid phase concentration
D_1	Diffusivity of Li^+ ions in the SEI
D_2	Diffusivity of anion in the SEI
D_{EFF}	Effective diffusivity in the SEI
D_{EC}	Diffusivity of ethylene carbonate in the SEI
D_s	Solid phase diffusivity
F	Faraday's constant
i_{APP}	Applied current density
i_{INT}	Anode intercalation current
i_{SEI}	Current in the SEI layer
j	Pore wall flux
k	Reaction rate constant
k_{SEI}	Reaction rate constant of SEI layer formation
l	Length of region
R_i	Radius of particle
R	Gas constant
T	Temperature
U	Open circuit potential
κ_{SEI}	Ionic conductivity of the SEI
ϕ	Solid phase potential
ϕ_{SEI}	Potential (drop) in the SEI

Lithium-ion batteries degrade due to several parasitic reactions that occur in the cell. These reactions cause loss of lithium inventory and loss of active material, leading to decreased capacity and increased resistance during repeated cell cycling. Physics-based battery models that include the governing equations for these fade mechanisms effectively predict cell aging and capacity loss. Adding these mechanisms can help researchers foresee the effect of various design parameters and operating conditions on cell performance.

There have been numerous efforts to model cell degradation in literature. The dominant mechanism chosen to capture capacity fade is the formation and growth of the solid electrolyte interphase (SEI) layer. The SEI layer forms due to the reduction of the electrolyte at the surface of the electrode particle and consists of several components of organic and inorganic species. The growth of this layer decreases the available lithium for intercalation, reducing the cell capacity. It also leads to increased resistance in the cell, which is linearly related to the thickness of the SEI.[1] Some of the other mechanisms that cause capacity fade include lithium plating, electrode particle cracking, SEI fracture, and electrolyte oxidation at the cathode.[2]

Commonly, the growth of the SEI layer is modeled with the Tafel equation that describes the electrolyte reduction reaction.[3–5] The growth can also be modeled to be solvent diffusion-limited. Solvent transport models typically predict a square root dependency for capacity fade with time.[6] Tang et al. analyzed the formation of the SEI layer by considering several proposed mechanisms, including solvent diffusion, electron migration, and electron tunneling. The rate-limiting mechanism depends on the porosity of the SEI.

Several models employ a mixed-mode,[7–10] where the parameters in the model determine whether the growth is a kinetically or diffusion-limited reaction. Safari et al. developed a multimodal model to predict aging that includes both the kinetic and diffusion-limited modes for the growth of the SEI layer.[7] In this work, the SEI layer resistance is a function of its thickness and fixed ionic conductivity. The effect of this resistance on the overpotential of both the main and side reactions is accounted for by using Ohm's law. Several simulation results by varying different parameters were obtained and analyzed to study the effect of kinetic or diffusion limitations on capacity fade. Kamyab et al. also proposed a mixed-mode model considering solvent diffusion through the SEI layer.[8] The study showed that employing a mixed-regime model can predict

*Electrochemical Society Fellow.
[z]E-mail: venkat.subramanian@utexas.edu

capacity loss accurately under constant voltage conditions. Electron conduction and tunneling have also been shown to be a rate-limiting step for the SEI layer growth. Single et al. showed that the rate-limiting step transitions from electron transport to solvent diffusion in the SEI at a specific critical porosity of the SEI.[9] In general, several factors can influence the resistance offered by the SEI layer, such as the equilibrium potential of the SEI formation reaction, the ionic conductivity of the SEI, structure, and composition of the SEI, etc.

A few studies have brought to light the effect of lithium ion concentration in the electrolyte within the SEI on ionic conductivity.[9,10] The transport of lithium ions plays a vital role in the SEI layer growth when the SEI is porous and thick.[9,11] The diffusion rate of lithium ions in the SEI affects the impedance of the SEI layer. Colclasure et al. showed that the fraction of lithium intercalated into the anode affects the potential across the SEI.[10] The study showed that the voltage loss due to the SEI layer growth should include the transport of lithium ions across the SEI layer and the resistance of the SEI layer should not be treated as a constant. Das et al. modeled the transport of lithium ions and electrons across the SEI where the ionic conductivity is proportional to the concentration of lithium ions within the SEI. The exchange current density for the SEI reaction was assumed to depend on the concentration of the ions and electrons in the SEI. The study showed that the resistance of the SEI is a function of several factors such as the cell potential, the electron concentration, the ion absorption energy, etc.[11] Christensen et al. modeled lithium ion and electron diffusion using dilute solution theory for the flux of the species, and the Laplace equation for the potential in the film.[12] As film thickness increases, the concentration polarization increases, but the rate of increase falls off. This is due to the transition from kinetic to diffusion limited growth. Phul et al. also used dilute solution theory to study the effect of potential drop across the SEI layer on capacity fade, with the potential drop being treated to be a constant with time. They observed an increase in capacity fade with an increase in potential drop until a certain value, after which the increase in capacity fade declined.[13]

This work details an approach to predict the growth of the SEI layer that may be limited by the transport of lithium ions in the SEI, and the effects of non-uniform lithium ion concentration in the SEI on capacity fade and increase in cell resistance. The SEI layer growth is modeled as a moving interface. Several researchers have modeled various electrochemical phenomena such as lithium electrodeposition in lithium metal batteries or transition metal dissolution in cathode materials as a moving boundary.[14–17] The expressions for lithium ion concentration in the SEI is used to derive an equation for the potential drop across the SEI layer under realistic conditions during long-term cycling and study its effect on the performance and capacity fade of a given lithium-ion battery.

Model Description

The growth of the SEI layer on a graphite particle at the anode is coupled with the single particle model (SPM) for a full cell simulation to study its influence on the capacity fade. The growth is modeled as the reduction of the solvent on the surface of a single electrode particle, assuming growth is uniform across all the particles. As the cell is cycled, this side reaction causes the layer to increase in thickness and affects the amount of lithium that can reach the particle surface for intercalation. In this study, we consider ethylene carbonate (EC) to be reacting with lithium ions leading to the formation of the SEI layer, as shown below.

$$(CH_2O)_2CO + 2e^- + 2Li^+ \rightarrow Li_2CO_3\downarrow$$

The mass transport flux, in terms of diffusion and migration inside the SEI layer, after using the Nernst-Einstein relation for each of the ionic species as well as the solvent is given as

$$N_i = -D_i \frac{\partial c_i}{\partial x} - z_i \frac{D_i F}{RT} c_i \frac{\partial \phi}{\partial x} \quad [1]$$

where i represents one of the species (1: Li^+ ions, 2: Anion, 3: Solvent) in the system. N is the flux for a given species in mol m^{-2}, D is the diffusivity, z is the charge, c is the concentration of the species, and ϕ is the electrostatic potential drop across the SEI layer. In this paper, ϕ can represent the potential drop across the SEI layer as well as the potential at the SEI/electrode interface itself, as the reference potential at the SEI/electrolyte is set to 0.

The mass balance for any species is given as

$$\frac{\partial c_i}{\partial t} = -\frac{\partial N_i}{\partial x} \quad [2]$$

If the SEI layer is taken to be a dilute solution, the assumption of electroneutrality for the binary system of ions is given as

$$\sum_i z_i c_i = 0 \quad [3]$$

The electroneutrality assumption for this system ($z_1 = 1$, $z_2 = -1$) results in $c_1 = c_2 = c$. The applied current density is related to the flux of the ionic species as

$$F \sum_i z_i N_i = -i_{APP} \quad [4]$$

where i_{APP} is the applied current density to the cell.

The potential across the SEI layer can be calculated by substituting Eqs. 1 and 3 in Eq. 4 and solving for ϕ (termed as ϕ_{SEI} in this work).,

$$\frac{d\phi_{SEI}}{dx} = -\frac{RT}{cF}\frac{(D_1 - D_2)}{(D_1 + D_2)}\frac{\partial c}{\partial x} + \frac{RT}{cF^2}\frac{i_{APP}(t)}{(D_1 + D_2)} \quad [5]$$

With the boundary condition setting the reference potential at the SEI layer/electrolyte interface.

$$\phi_{SEI}|_{x=s_{SEI}(t)} = 0$$

Equation 5 expresses the potential across the SEI as a function of the concentration and concentration gradient of the lithium ions in the SEI. The potential drop across the SEI layer influences the overpotential of the intercalation at the negative electrode. In literature, the potential drop due to the SEI layer growth is generally treated as an ohmic loss, given by the resistance of the SEI layer times the current applied at the particle surface. The resistance of the SEI layer is a function of its thickness and ionic conductivity.

Substituting Eq. 5 in 2, the governing equations for the ionic transport in the SEI is given as

$$\frac{\partial c_i}{\partial t} = D_{EFF}\frac{\partial^2 c_i}{\partial x^2}$$
$$D_{EFF} = \frac{2D_1D_2}{D_1 + D_2} \quad [6]$$

The equations governing the solvent transport can be determined using Eq. 1, taking it to be a neutral species with no contribution to charge.

$$\frac{\partial c_{EC}}{\partial t} = D_{EC}\frac{\partial^2 c_{EC}}{\partial x^2} \quad [7]$$

Equation 6 governs the transport of the ionic species, and Eq. 7 is for the solvent within the SEI layer. Hereafter, the concentration of lithium ions is noted as c, and the solvent concentration is indicated as c_{EC}. The boundary conditions for the lithium ions and the solvent are given as:

$$At\ x = 0: -D_1 \frac{\partial c}{\partial x}\bigg|_{x=0} = \frac{i_{APP}(t)}{2F}$$
$$-D_{EC} \frac{\partial c_{EC}}{\partial x}\bigg|_{x=0} = \frac{i_{SEI}(t)}{F}$$

$$At\ x = s_{SEI}(t): c|_{x=s_{SEI}(t)} = c_0$$
$$c_{EC}|_{x=s_{SEI}(t)} = \varepsilon c_e$$

where i_{SEI} is the side reaction or SEI layer growth current density in A m^{-2}, and $s_{SEI}(t)$ is the thickness of the SEI layer. ε represents the "porosity" of the SEI, where ε can be understood as a partition coefficient between the SEI and the electrolyte.[7]

In the absence of concentration gradient across the SEI layer, the conductivity of the SEI layer can be evaluated as[18]

$$\kappa = \frac{F^2 c_0}{RT}(D_1 + D_2) \quad [8]$$

Assuming the diffusivities D_1 and D_2 to be equal, Eq. 5 is employed to observe the effect of the ion transport across the SEI layer, and its influence on the overall battery capacity fade and resistance.

The growth of the SEI layer (s_{SEI}) is captured by considering the SEI layer/electrolyte interface as a moving boundary, with the velocity given by

$$\frac{ds_{SEI}}{dt} = \frac{i_{SEI}(t)}{2F}\frac{M_w}{\rho} \quad [9]$$

These equations are integrated with the SPM equations to model a full lithium-ion cell. Table I summarizes the equations commonly used in literature to model the growth of the SEI layer. This work aims to compare the predictions from well-known models in literature (named Model 1), and the proposed model (Model 2). Model 1 comprises of Eq. 7 for modeling solvent diffusion in the SEI, Eq. 9 for the growth of the SEI layer and equations for modeling the reduction reaction, shown in Table I. The potential drop is expressed as $\frac{s_{SEI}(t)}{\kappa} i_{APP}(t)$ for Model 1. This expression for the potential drop represents the ohmic drop due to the growth of the SEI layer. The potential drop in Model 2 is described by Eq. 5 and is a function of the concentration of lithium ions in the SEI layer.

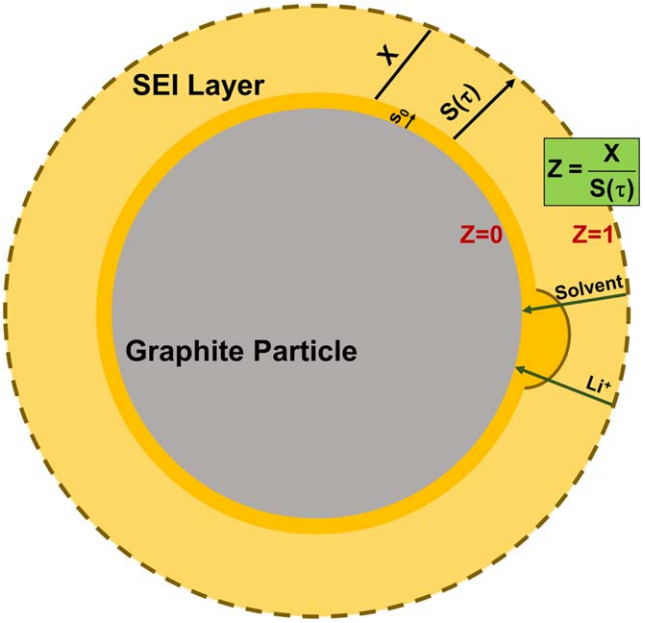

Figure 1. Schematic of the Solid Electrolyte Interphase (SEI) layer on the surface of the graphite particle, including the coordinate system explained in this work.

To account for the fact that the SEI layer is growing, and the SEI layer/electrolyte interface is moving, a coordinate transformation is applied to the transport equations to freeze the coordinates from a moving frame to a stationary frame, as shown in Fig. 1. The transformation, known as the Landau transformation, is given as

$$Z = \frac{X}{S(\tau)} \quad [10]$$

where $S(\tau) = \frac{s_{SEI}}{s_0}$, $X = \frac{x}{s_0}$ and $\tau = \frac{R_{pn}}{D_1}$.

s_0 is the initial thickness of the SEI layer after the formation cycles.

Using the transformed variable Z, $C = \frac{c}{c_0}$ and $C_{EC} = \frac{c_{EC}}{c_0}$, Eq. 6 can be rewritten as:

Table I. Summary of the governing equations from Model 1 and Model 2 for the SEI layer growth.

Governing Equations	Boundary Condition
Model 1:	
Solvent Transport: $\frac{\partial c_{EC}}{\partial t} = D_{EC}\frac{\partial^2 c_{EC}}{\partial x^2} + \frac{ds_{SEI}}{dt}\frac{\partial c_{EC}}{\partial x}$	$-D_{EC}\frac{dc_{EC}}{dx}\Big\|_{x=0} = -\frac{i_{SEI}(t)}{F} + \frac{ds_{SEI}}{dt}c_{EC}$ $c_{EC}\|_{x=s(t)} = \varepsilon c_e$
Growth of the SEI Layer: $\frac{ds_{SEI}}{dt} = \frac{i_{SEI}(t)}{2F}\frac{M_w}{\rho}$ *Side Reaction Current:* $i_{SEI}(t) = Fk_{SEI}c_{EC}\exp\left(-\frac{0.5F}{RT}(\phi_n - U_{SEI} - \phi_{SEI})\right)$ Where $\phi_{SEI} = \frac{s_{SEI}}{\kappa} i_{APP}$	
Model 2:	
Li^+ Transport: $\frac{\partial c}{\partial t} = D_{EFF}\frac{\partial^2 c}{\partial x^2}$	$-D_1\frac{dc}{dx}\Big\|_{x=0} = \frac{i_{APP}(t)}{2F}$ $c\|_{x=s(t)} = c_0$
Solvent Transport: $\frac{\partial c_{EC}}{\partial t} = D_{EC}\frac{\partial^2 c_{EC}}{\partial x^2}$	$-D_{EC}\frac{dc_{EC}}{dx}\Big\|_{x=0} = \frac{i_{SEI}(t)}{F}$ $c_{EC}\|_{x=s(t)} = \varepsilon c_e$
Potential in the SEI Layer: $\frac{d\phi_{SEI}}{dx} = -\frac{RT}{cF}\frac{(D_1 - D_2)}{(D_1 + D_2)}\frac{\partial c}{\partial x} + \frac{RT}{cF^2}\frac{i_{APP}(t)}{(D_1 + D_2)}$	$\phi_{SEI}\|_{x=s(t)} = 0$

Table II. List of governing equations for the SEI layer for Model 2 after Landau Transformation.

Governing Equations	Boundary Condition	Equations after Landau Transform	Boundary Condition after Landau Transform
$\frac{\partial c}{\partial t} = D_{EFF}\frac{\partial^2 c}{\partial x^2}$	$-D_1\frac{dc}{dx}\Big\|_{x=0} = \frac{i_{APP}(t)}{F}$	$\frac{\partial C}{\partial \tau} = \frac{1}{S(\tau)^2}\frac{\partial^2 C}{\partial Z^2} + \frac{dS}{d\tau}\frac{Z}{S(\tau)}\frac{\partial C}{\partial Z}$	$\frac{\partial C}{\partial Z}\Big\|_{Z=0} = \frac{\delta}{2}S(\tau)$
	$c(x,t)\|_{x=s(t)} = c_0$		$C_1\|_{Z=1} = 1$
$\frac{\partial c_{EC}}{\partial t} = D_{EC}\frac{\partial^2 c_{EC}}{\partial x^2}$		$-D_{EC}\frac{dc_{EC}}{dx}\Big\|_{x=0} = \frac{i_{SEI}(t)}{F}$	$\frac{\partial C_{EC}}{\partial \tau} = \frac{1}{S(\tau)^2}\frac{\partial^2 C_{EC}}{\partial Z^2} + \frac{dS}{d\tau}\frac{Z}{S(\tau)}\frac{\partial C_{EC}}{\partial Z}$
$\frac{\partial C_{EC}}{\partial Z}\Big\|_{Z=0} = \delta_{SEI}S(\tau)\left(\frac{D_1}{D_{EC}}\right)$			
	$c_{EC}\|_{x=s(t)} = \varepsilon c_e$		$C_{EC}\|_{Z=1} = \varepsilon\frac{c_e}{c_0}$
$\frac{d\phi_{SEI}}{dx} = -\frac{RT}{cF}\frac{(D_1-D_2)}{(D_1+D_2)}\frac{\partial c}{\partial x} + \frac{RT}{cF^2}\frac{i_{APP}}{(D_1+D_2)}$	$\phi_{SEI}\|_{x=s(t)} = 0$	$\frac{\frac{\partial \phi_{SEI}}{\partial Z}}{S(\tau)} = -\frac{RTL}{CFS(\tau)}\left(\frac{D_2-D_1}{D_1+D_2}\right)\frac{\partial C}{\partial Z} + \frac{RT\delta D_1}{C_1F(D_1+D_2)}$	At $Z=1$: $\phi\|_{Z=1} = 0$
$i_{SEI} = Fk_{SEI}c_{EC}\exp\left(-\frac{0.5F}{RT}(\phi_n - U_{SEI} - \phi_{SEI})\right)$			

$$\frac{\partial C_i}{\partial \tau} = \frac{1}{S(\tau)^2}\frac{\partial^2 C_i}{\partial Z^2} + \frac{dS}{d\tau}\frac{Z}{S(\tau)}\frac{\partial C_i}{\partial Z} \quad [11]$$

The transformed boundary conditions are:

$$At\ Z=0:\ \frac{\partial C}{\partial Z}\Big|_{Z=0} = \frac{-i_{APP}s_0S(\tau)}{2FD_1c_0} = \frac{\delta}{2}S(\tau)$$

$$\frac{\partial C_{EC}}{\partial Z}\Big|_{Z=0} = \frac{-i_{SEI}s_0S(\tau)}{FD_1c_0}\left(\frac{D_1}{D_{EC}}\right) = \delta_{SEI}S(\tau)$$

$$At\ Z=1:\ C|_{Z=1} = 1$$

$$C_{EC}|_{Z=1} = \frac{\varepsilon c_e}{c_0}$$

where $\delta = -\frac{i_{APP}s_0}{FD_1c_0}$ is the applied current density in dimensionless form, and $\delta_{SEI} = -\frac{i_{SEI}s_0}{FD_1c_0}$ is the side reaction current density in dimensionless form.

In terms of Z, the equation for the potential drop (Eq. 5) across the electrolyte can be rearranged as:

$$\frac{\frac{d\phi}{dZ}}{S(\tau)} = -\frac{RTF}{CF^2S(\tau)}\left(\frac{D_2-D_1}{D_1+D_2}\right)\frac{\partial C}{\partial Z} + \frac{RT\delta D_1}{CF(D_1+D_2)} \quad [12]$$

The boundary condition for the potential ϕ is:

$$\text{At } Z=1:\ \phi|_{Z=1} = 0$$

The initial conditions for the given system are considered as $C(Z,\ 0) = 1$, $C_{EC}(Z,\ 0) = \frac{\varepsilon c_e}{c_0}$ and $\phi(Z,\ 0) = 0$.

Table II summarizes the partial differential equations in the system in the original coordinate and the transformed coordinates.

The above equations were first discretized spatially using the finite difference method and later with orthogonal collocation in x for convergence. These equations are a set of differential-algebraic equations (DAEs) that describe the complete system. The parameters used for this model are listed in Table III. The discretized equations were solved in Maple with its stiff solver aided by consistent initialization for algebraic variables using the approach by Lawder et al.[19]

Results and Discussion

The simulations were conducted with a constant current discharge followed by a constant current (CC) at C/2 rate and a constant voltage (CV) charging protocol. The model proposed (Model 2) was compared to the model reported in the literature (Model 1) for capacity predictions. Model 1 includes convective transport in the governing equations and boundary conditions, whereas model 2 uses Landau transform to model the moving boundary due to the SEI layer growth. This section focuses on comparing the two models based on their predictions under different scenarios.

Table III. List of Parameters.

Symbol (i = n,p)	Parameter	Negative Electrode	Positive Electrode	Units
k_i	Reaction Rate Constant	5.031×10^{-11}	2.334×10^{-11}	$m^{2.5}/mol^{0.5}s$
D_{si}	Solid Phase Diffusivity	3.9×10^{-14}	1×10^{-14}	$m^2\ s^{-1}$
R_{pi}	Radius of Particle	2×10^{-6}	2×10^{-6}	m
$c_{si(max)}$	Maximum concentration at particle surface	30555	51555	mol m^{-3}
e_i	Porosity	0.485	0.385	
e_{fi}	Filler Fraction	0.0326	0.025	
l_i	Region Thickness	88×10^{-6}	80×10^{-6}	m
	SEI Parameters			
k_{SEI}	Reaction Rate Constant	5.0887×10^{-6}[a]		m/s
c_0	Bulk Salt Concentration	1000[a]		mol m^{-3}
c_e	Bulk Solvent Concentration	4541[a]		mol m^{-3}
D_{EC}	Solvent Diffusivity	2×10^{-19}[c]		$m^2\ s^{-1}$
M_{SEI}	Molecular Mass	0.07389[a]		kg mol^{-1}
ρ_{SEI}	Density	2110 [a]		kg m^{-3}
s_0	Initial SEI Thickness	5×10^{-9}[b]		m

a) Kindermann et al.[20] b) Safari et al.[7] c) Crawford et al.[21]

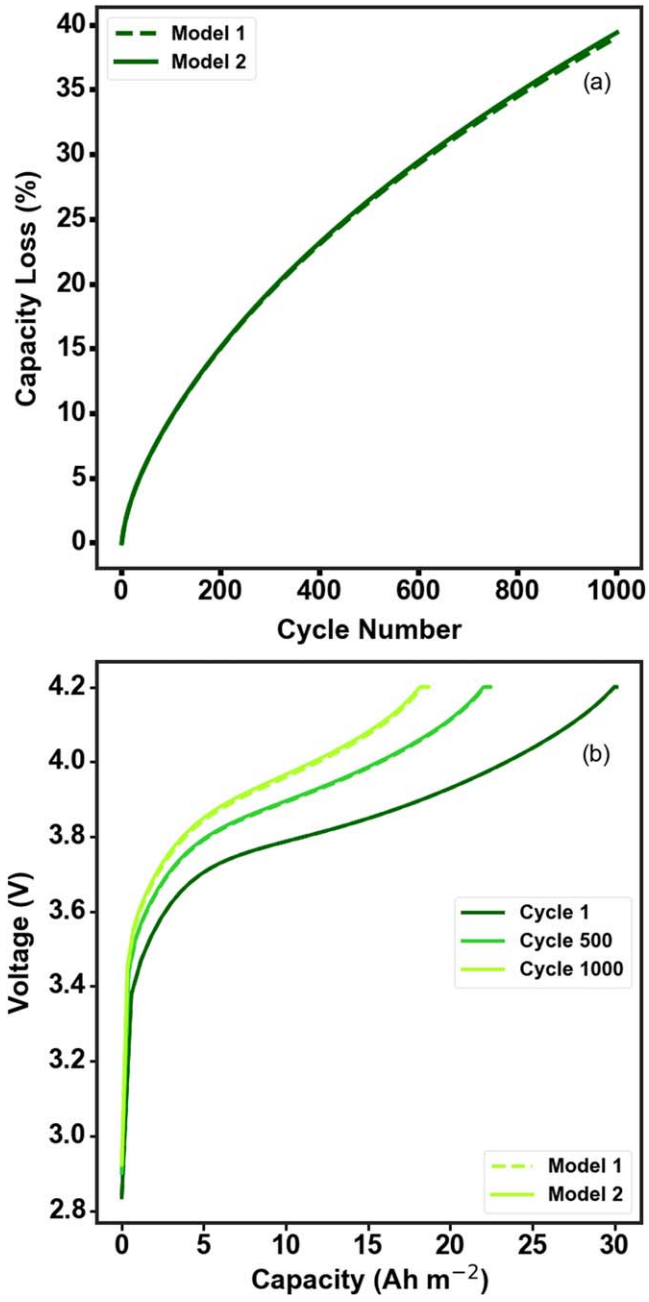

Figure 2. (a) Comparison of the charge capacity prediction v/s cycle number from Model 1 and Model 2. (b) Comparison of voltage predictions during CC + CV charge for three different cycles from Model 1 and Model 2.

Figure 2a shows the comparison of predicted capacity after cycling for the two different models. There is little difference between the predictions for capacity between the two models, with only 0.36% difference in capacity loss after 1000 cycles. Similarly, the voltage predictions for different cycles are comparable, as seen in Fig. 2b. There is a slight variation in predictions with increasing cycle number, approximately a 4 mV difference between predictions. These results were obtained using the baseline parameters given in Table III. Next, we will consider and analyze scenarios where predictions from the two models differ. In general, Model 2 captures the effect of lithium ion concentration gradient on the potential drop across the SEI layer, leading to larger overpotential and lesser usable capacity.

Poor lithium ion transport in the SEI.—The potential drop across the SEI is influenced by the local concentration of the lithium ions that transport through the interphase. Generally, the concentration of lithium ions across the SEI layer thickness remains largely uniform, making constant ionic conductivity a reasonable assumption. However, certain conditions can lead to sufficient mass transport limitation resulting in significant concentration variation within the SEI, making the constant ionic conductivity assumption invalid. One condition under which this may happen would be low lithium ion diffusivity in the SEI. Low temperature operation and electrolyte composition are some of the critical factors that can slow down lithium ion diffusion in the SEI.[22]

Table IV. List of ionic conductivities in the SEI and their corresponding lithium ion diffusivities.

Li^+ Ionic Conductivity, κ_{SEI} (S m^{-1})	Li^+ Diffusivity, D_1 (m^2 s^{-1})
1.265×10^{-5}	1.684×10^{-15}
2.3×10^{-6} a)	3.062×10^{-16} (D_{1_0})
1.265×10^{-6}	1.684×10^{-16}

a) Fu et. al.[24]

For the first case study, the diffusivities of the anion and cation were taken to be equal for simplification. Using this assumption and Eq. 8, the diffusivity of the lithium ions (D_1) and corresponding ionic conductivity of the SEI can be determined. Table IV shows the different values of lithium ion diffusivity along with corresponding ionic conductivities of the SEI. The values of lithium ion diffusivity in the SEI are in agreement with the values observed in the literature for Li_2CO_3.[23]

Figure 3a shows the potential drop across the SEI layer predicted by the two different models for the different diffusivities shown in Table IV, which increases in magnitude as the diffusivity decreases. The lithium ion concentration at the SEI/Electrode interface as well as within the SEI goes down with cycling due to the increased SEI thickness slowing down the transport of lithium ions. This effect becomes more prominent for SEI with low diffusivity, as seen in Fig. 3b. This trend correlates well with the trend observed in potential drop across the SEI predicted by Model 2. Both Models 1 and 2 predict an increase in potential drop across the SEI with cycling as well as with lowering the diffusivity. Since Model 1 assumes constant ionic conductivity by ignoring the concentration gradient within the SEI, it fails to account for the effect of the same on the potential drop in the SEI layer. This may lead to significant underprediction in potential drop under severally mass transport limited conditions in the SEI. On the other hand, Model 2 predicts a higher potential drop than Model 1, with the difference becoming larger with decreasing diffusivity.

The potential drop across the SEI layer is related to the concentration of lithium ion within the SEI and at the SEI/particle interface. Under the conditions which lead to a large concentration gradient within SEI, the lithium ion concentration at the SEI/particle interface can be much lower than the bulk concentration, which may lead to a high potential drop across the SEI. This effect becomes more prominent for SEI with lower diffusivity. With lowering of diffusivity of lithium ions in the SEI, the potential calculated from the two models deviates with the magnitude of the potential drop increasing rapidly when computed using the proposed new model (Model 2) This can be further understood by considering the effective ionic conductivity. Effective ionic conductivity is related to the local lithium ion concentration. As the lithium ion concentration decreases due to mass transport limitations, the effective conductivity also decreases. Thus, the total SEI resistance increases not only due to the increase in its thickness as considered in Model 1, but also due to decreasing effective ionic conductivity as captured by Model 2. As a result, Model 2, employing a more accurate approach, predicts higher resistance and resulting potential drop. Figures 3d and 3e show the variations in potential and concentration across the thickness of the SEI layer at cycle 1000. The trend in the concentration variations within the SEI layer reflects in the potential drop across the SEI layer. The potential drop across the SEI layer becomes non-linear as the ion diffusivity decreases. It should be noted that the magnitude of the potential in SEI plotted across the SEI thickness provides the potential drop in the SEI as the reference potential is set at the SEI/electrolyte interface.

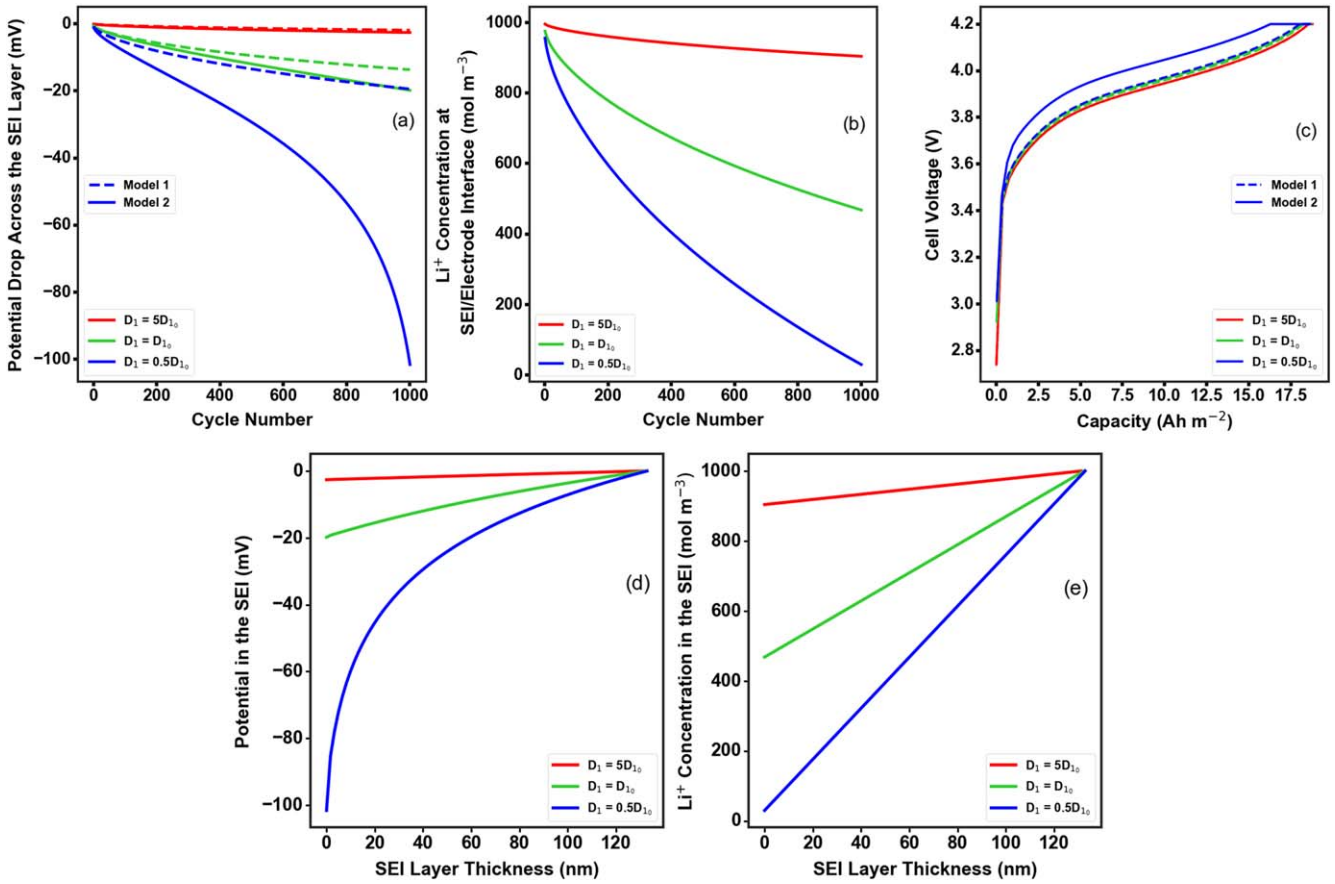

Figure 3. (a) Comparison of potential drop predictions v/s cycle number for three different values of lithium ion diffusivities, D_1 (corresponding κ_{SEI} was used for model 1's predictions from Model 1 and Model 2. (b) Concentration of lithium ions at the electrode/SEI interface for three different values of lithium ion diffusivities, D_1. (c) The voltage response at cycle 1000 for different lithium ion diffusivities. (d) The potential drop and (e) concentration of lithium ions across the SEI layer thickness for three different values of lithium ion diffusivities, D_1.

To further illustrate the model's predictions with low diffusivities, a comparison of several features from both the models is shown in Fig. 4 for different diffusivities at cycle 1000. The magnitude of the potential drop predicted from this work (Model 2) increases exponentially with cycles/time in the case of poor diffusion. In comparison, the model reported in the literature (Model 1) shows a linear increase and at a lower rate than predicted by Model 2. This trend also leads to a divergence between the two models in capacity (usable) predictions at the lower diffusivity, as shown in Fig. 4a. As discussed earlier, the effective ionic conductivity of the film decreases as the lithium ion concentration decreases during cycling. This results in an increase in the film resistance, which in turn leads the cell voltage to reach its cutoff (specified as 4.2 V in the simulations) quicker, as shown in Fig. 4b. Model 2 predicts high concentration polarization that results in a shorter constant current charging phase which would imply longer charging to charge the battery to a specific state of charge (SOC) in a practical scenario.

Figure 4c shows the SEI layer thickness predicted by both models for the different diffusivity values considered. There is very little difference in the thickness of the SEI layer predicted by the two models over a wide range of diffusivity values, suggesting very similar predictions of loss of lithium inventory. However, the capacity loss predictions differ significantly, with Model 2 showing a much higher capacity loss for the smallest diffusivity value considered. This can be attributed to the much higher and accurate prediction of the potential drop across SEI by Model 2, leading to less usable capacity for the charging rate and protocol considered.

The results above were simulated with the assumption that the diffusivities of the cation and anion species were equal. This means that the potential drop across the SEI layer is a function of the concentration of lithium ions. When this assumption is relaxed, the potential drop becomes a function of both the concentration as well as the concentration gradient of lithium ions. Even for a very simple 1D model, the convection term for the concentration equation is challenging to solve. Brute force discretization gives oscillations in the numerical simulation. This will be discussed in a later paper, and it is sufficient to state that when D_1 is not equal to D_2, the moving boundary growth has a higher impact.

Effect of C-rate on potential drop across the SEI Layer.— Figure 5a shows the potential drop with the time over 300 charge/discharge cycles at different C-rates. Since higher current leads to higher potential drop, the increase in potential drop with increase in C-rate is expected. In Model 1, the concentration of lithium ions in the SEI is assumed to be uniform which results in constant ionic conductivity for the SEI. This leads to only linearly increasing potential drop due to the ohmic relationship between current and potential. Model 2 accounts for the nonuniform concentration in the SEI due to the mass transport limitation by solving the underlying mass transport equation. As a result, Model 2 predicts a much higher potential drop across SEI, especially under severely mass transport limited conditions, which may occur during high C-rate constant charging operation. The difference between the potential drop predicted by the two models increases dramatically with the increase in C-rate. A consequence of this would be a higher loss in usable capacity predicted by Model 2 compared to Model 1 for fixed total charging time, as shown in Fig. 5b. Thus, Model 2 can lead to significant improvement in the prediction accuracy for the life of the battery at high rates. It should also be noted that the capacity loss is the highest for the lowest C-rate as per both the models. Figure 5c

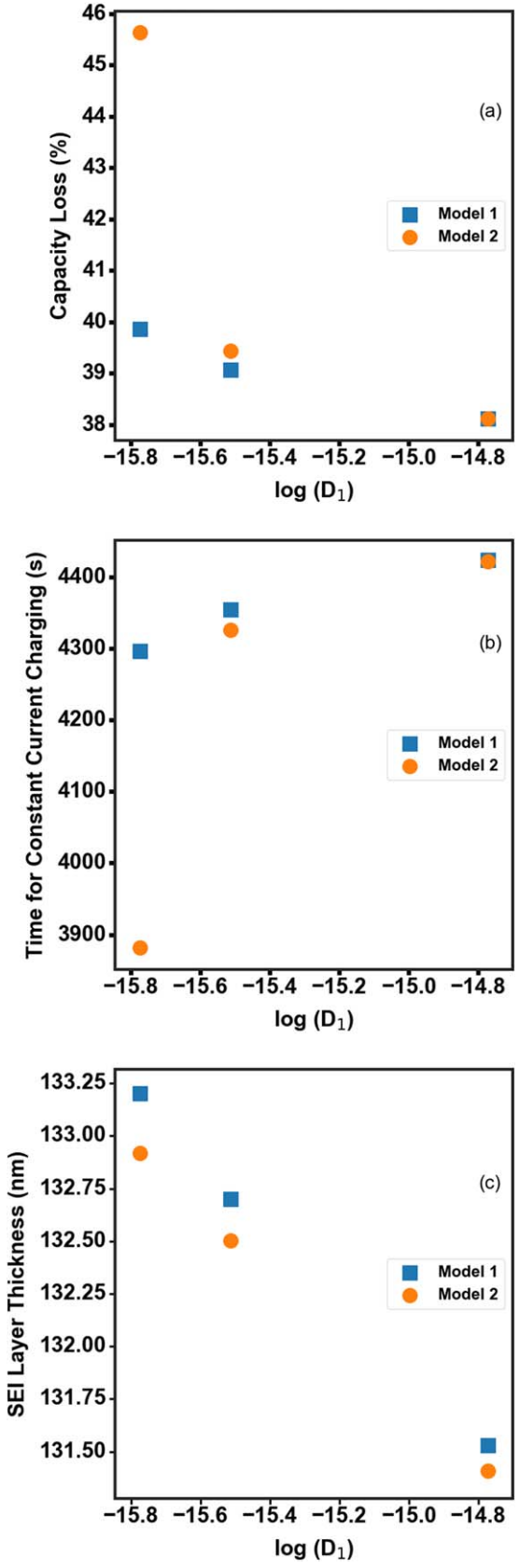

Figure 4. (a) Capacity loss predictions from Model 1 and Model 2 at cycle 1000 for different lithium ion diffusivities. (b) The time taken for constant current charging calculated from Model 1 and Model 2 at cycle 1000 for different lithium ion diffusivities. (c) The SEI layer thickness predictions from Model 1 and Model 2 at cycle 1000 for different lithium ion diffusivities.

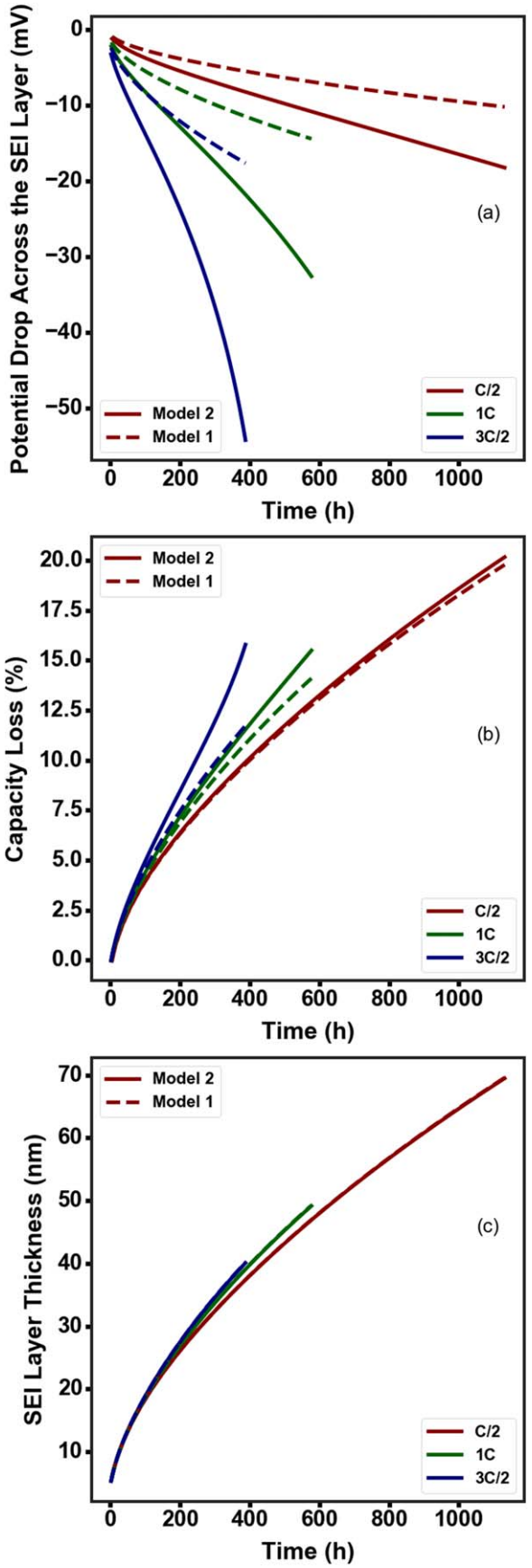

Figure 5. (a) Potential drop predictions (b) Capacity loss predictions (c) SEI layer thickness predictions from Model 1 and Model 2 at different C-rates for 300 cycles.

shows the predictions of the SEI layer thickness between the two models. Like the results in Fig. 4c for different ion diffusivities, the predictions for the SEI layer thickness between the two models are close to each other. This shows that the difference in potential drop and capacity predicted from the two models comes from the resistance increase in the SEI stemming from the transport limitations. Model 1 considers the resistance of the SEI layer to be a function of the SEI layer thickness and the conductivity of the SEI. In contrast, Model 2 considers the effect of ion and solvent transport on the resistance increase that leads to capacity fade.

Conclusions

We studied the effect of moving interface in capacity fade models reported in the literature. A coordinate transformation approach was used to model the growth of the SEI layer on the surface of the electrode particle. The model includes transport of lithium ions giving it the ability to capture concentration-dependent resistance offered by the SEI, specifically relevant under transport limited conditions. The model was compared to the widely used capacity fade model considering SEI formation reported in literature, where the SEI layer conductivity is considered to be a constant value. Instead of rigorously derived mathematical formulation for moving boundary, the models in literature include convective transport of species in the SEI. The model presented in this work overcomes these issues by using dilute solution theory for modeling the transport of ions in the SEI and applying the landau transform to treat the moving boundary in a mathematically rigorous manner. We demonstrate unique prediction capabilities of the model by studying effect of ion diffusivity in the SEI and show that for low ion diffusivities in the SEI, the potential drop across the SEI escalates due to the concentration gradient within the SEI and depletion of lithium ions at the electrode/SEI interface. Similar finding is also observed and reported for different C-rates. Finally, the usable capacity has been studied using the proposed model under mass transport limited conditions, both due to low ion diffusivity and high C-rate. The results on capacity prediction show that higher potential drop in the SEI predicted by the proposed model lead to higher capacity loss in terms of the usable capacity. This capacity loss is attributed to the higher resistance of the cell predicted by the proposed model. Future work includes researching the effect of other parameters that influence the formation and growth of the SEI, such as the equilibrium potential of the SEI formation. This model can also be used to study the interplay of other degradation mechanisms such as Mn dissolution, lithium plating, etc., on the SEI layer growth. The effect of ion transport in the SEI can be studied with a battery model with higher fidelity, such as the Tank-in Series or the P2D model. These models can assist in understanding these effects across the electrode thickness.

The codes used in this work will be posted online, on the corresponding author's website. (http:/sites.utexas.edu/maple).

Acknowledgments

This work at the University of Texas at Austin was supported by U.S. DOE Office of Electricity award DEAC05–76RL01830 through PNNL subcontract 475525.

Appendix A

A.1. SPM model equations.—Negative Electrode:

$$\frac{\partial c_{sn}}{\partial t} = D_{sn}\left(\frac{\partial^2 c_{sn}}{\partial x^2} + \frac{2}{x}\frac{\partial c_{sn}}{\partial x}\right)$$

$$\left.\frac{\partial c_{sn}}{\partial x}\right|_{x=0} = 0$$

$$\left. D_{sn}\frac{\partial c_{sn}}{\partial x}\right|_{x=R_{pn}} = \frac{i_{INT}(t)}{F}$$

$$j_n = \frac{-i_{INT}(t)}{a_n l_n F}$$

$$j_n = 2k_n\sqrt{c}\sqrt{(c_{sn(\max)} - c_{sn}(R_{pn}, t))}\sinh\left(\frac{0.5F}{RT}(\phi_n - U_n - \phi_{SEI})\right)$$

Positive Electrode:

$$\frac{\partial c_{sp}}{\partial t} = D_{sp}\left(\frac{\partial^2 c_{sp}}{\partial x^2} + \frac{2}{x}\frac{\partial c_{sp}}{\partial x}\right)$$

$$\left.\frac{\partial c_{sp}}{\partial x}\right|_{x=0} = 0$$

$$\left. D_{sp}\frac{\partial c_{sp}}{\partial x}\right|_{x=R_{pp}} = \frac{i_{APP}(t)}{F}$$

$$j_p = \frac{i_{APP}(t)}{a_p l_p F}$$

$$j_p = 2k_p\sqrt{c_0}\sqrt{(c_{sp(\max)} - c_{sp}(R_{pp}, t))}\sinh\left(\frac{0.5F}{RT}(\phi_p - U_p)\right)$$

Cell Level Equations:

$$i_{APP}(t) = i_{INT}(t) + i_{SEI}(t)$$

$$V(t) = \phi_p - \phi_n$$

$$Q(t) = \int_0^t \frac{i_{APP}(t)}{3600}$$

The empirical expressions for the open-circuit voltage are given as:

Negative Graphite Electrode:

$$U_n = 0.7222 + 0.1387\left(\frac{c_{sn}}{c_{sn(\max)}}\right) + 0.029\left(\frac{c_{sn}}{c_{sn(\max)}}\right)^{1/2} - 0.0172\left(\frac{c_{sn}}{c_{sn(\max)}}\right)^{-1} + 0.0019\left(\frac{c_{sn}}{c_{sn(\max)}}\right)^{-3/2} + 0.2808\exp\left(0.9 - 1.5\left(\frac{c_{sn}}{c_{sn(\max)}}\right)\right) - 0.7984\exp\left(0.4465\left(\frac{c_{sn}}{c_{sn(\max)}}\right) - 0.4108\right)$$

Positive LCO Electrode:

$$U_p = \frac{-4.656 + 88.669\left(\frac{c_{sp}}{c_{sp(\max)}}\right)^2 - 401.119\left(\frac{c_{sp}}{c_{sp(\max)}}\right)^4 + 342.909\left(\frac{c_{sp}}{c_{sp(\max)}}\right)^6 - 462.471\left(\frac{c_{sp}}{c_{sp(\max)}}\right)^8 + 433.434\left(\frac{c_{sp}}{c_{sp(\max)}}\right)^{10}}{-1 + 18.933\left(\frac{c_{sp}}{c_{sp(\max)}}\right)^2 - 79.532\left(\frac{c_{sp}}{c_{sp(\max)}}\right)^4 + 37.311\left(\frac{c_{sp}}{c_{sp(\max)}}\right)^6 - 73.083\left(\frac{c_{sp}}{c_{sp(\max)}}\right)^8 + 95.96\left(\frac{c_{sp}}{csp_{(\max)}}\right)^{10}}$$

ORCID

Maitri Uppaluri https://orcid.org/0000-0002-6612-3009
Krishna Shah https://orcid.org/0000-0002-7802-6361
Vilayanur Viswanathan https://orcid.org/0000-0003-1319-7984
Venkat R. Subramanian https://orcid.org/0000-0002-2092-9744

References

1. E. Peled, *J. Electrochem. Soc.*, **126**, 2047 (1979).
2. J. M. Reniers, G. Mulder, and D. A. Howey, *J. Electrochem. Soc.*, **166**, A3189 (2019).
3. P. Ramadass, B. Haran, P. M. Gomadam, R. White, and B. N. Popov, *J. Electrochem. Soc.*, **151**, 196 (2004).
4. M. Tang, S. Lu, and J. Newman, *J. Electrochem. Soc.*, **159**, A1775 (2012).
5. T. R. Ashwin, Y. M. Chung, and J. Wang, *J. Power Sources*, **328**, 586 (2016).
6. H. J. Ploehn, P. Ramadass, and R. E. White, *J. Electrochem. Soc.*, **151**, A456 (2004).
7. M. Safari, M. Morcrette, A. Teyssot, and C. Delacourt, *J. Electrochem. Soc.*, **156**, 145 (2009).
8. N. Kamyab, J. W. Weidner, and R. E. White, *J. Electrochem. Soc.*, **166**, A334 (2019).
9. F. Single, B. Horstmann, and A. Latz, *J. Electrochem. Soc.*, **164**, E3132 (2017).
10. A. M. Colclasure, K. A. Smith, and R. J. Kee, *Electrochim. Acta*, **58**, 33 (2011).
11. S. Das, P. M. Attia, W. C. Chueh, and M. Z. Bazant, *J. Electrochem. Soc.*, **166**, E107 (2019).
12. J. Christensen and J. Newman, *J. Electrochem. Soc.*, **151**A1977 (2004).
13. S. Phul, A. Deshpande, and B. Krishnamurthy, *Electrochim. Acta*, **164**, 281 (2015).
14. B. S. Vishnugopi, A. Verma, and P. P. Mukherjee, *J. Phys. Chem. C*, **124**, 16784 (2020).
15. C. H. Chen and C. W. Pao, *J. Power Sources*, **484**, 229203 (2021).
16. M. Uppaluri, A. Subramaniam, L. Mishra, V. Viswanathan, and V. R. Subramanian, *J. Electrochem. Soc.*, **167**, 160547 (2020).
17. A. Ghosh, J. M. Foster, G. Offer, and M. Marinescu, *J. Electrochem. Soc.*, **168**, 020509 (2021).
18. J. Newman and K. E. Thomas-Alyea, *Electrochemical Systems* (Wiley, Hoboken, NJ) 3rd ed. (2004).
19. M. T. Lawder, V. Ramadesigan, B. Suthar, and V. R. Subramanian, *Comput. Chem. Eng.*, **82**, 283 (2015).
20. F. M. Kindermann, J. Keil, A. Frank, and A. Jossen, *J. Electrochem. Soc.*, **164**, E287 (2017).
21. A. J. Crawford, D. Choi, P. J. Balducci, V. R. Subramanian, and V. V. Viswanathan, *J. Power Sources*, **501**, 230032 (2021).
22. O. Borodin, G. D. Smith, and P. Fan, *J. Phys. Chem. B*, **110**, 22773 (2006).
23. L. Benitez and J. M. Seminario, *J. Electrochem. Soc.*, **164**, E3159 (2017).
24. R. Fu, S. Y. Choe, V. Agubra, and J. Fergus, *J. Power Sources*, **278**, 506 (2015).